The Astrophysical Journal, 758:140 (8pp), 2012 October 20 doi:10.1088/0004-637X/758/2/140

FERMI OBSERVATIONS OF γ-RAY EMISSION FROM THE MOON

A. A. Abdo[1,65], M. Ackermann[2], M. Ajello[3], W. B. Atwood[4], L. Baldini[5], J. Ballet[6], G. Barbiellini[7,8], D. Bastieri[9,10], K. Bechtol[3], R. Bellazzini[5], B. Berenji[3], R. D. Blandford[3], E. Bonamente[11,12], A. W. Borgland[3], E. Bottacini[3], A. Bouvier[4], J. Bregeon[5], M. Brigida[13,14], P. Bruel[15], R. Buehler[3], S. Buson[9,10], G. A. Caliandro[16], R. A. Cameron[3], P. A. Caraveo[17], J. M. Casandjian[6], C. Cecchi[11,12], E. Charles[3], A. Chekhtman[1], J. Chiang[3], S. Ciprini[12,18], R. Claus[3], J. Cohen-Tanugi[19], J. Conrad[20,21,66], S. Cutini[22], F. D'Ammando[11,23,24], A. de Angelis[25], F. de Palma[13,14], C. D. Dermer[26], S. W. Digel[3], E. do Couto e Silva[3], P. S. Drell[3], A. Drlica-Wagner[3], R. Dubois[3], C. Favuzzi[13,14], S. J. Fegan[15], W. B. Focke[3], P. Fortin[15], Y. Fukazawa[27], S. Funk[3], P. Fusco[13,14], F. Gargano[14], N. Gehrels[28], S. Germani[11,12], N. Giglietto[13,14], P. Giommi[22], F. Giordano[13,14], M. Giroletti[29], T. Glanzman[3], G. Godfrey[3], G. A. Gomez-Vargas[30,31,32], I. A. Grenier[6], J. E. Grove[26], S. Guiriec[33], D. Hadasch[16], E. Hays[28], A. B. Hill[3,34], D. Horan[15], X. Hou[35], R. E. Hughes[36], G. Iafrate[7,37], M. S. Jackson[21,38], G. Jóhannesson[39], A. S. Johnson[3], T. Kamae[3], H. Katagiri[40], J. Kataoka[41], J. Knödlseder[42,43], M. Kuss[5], J. Lande[3], S. Larsson[20,21,44], L. Latronico[45], M. Lemoine-Goumard[46,67], F. Longo[7,8], F. Loparco[13,14], B. Lott[46], M. N. Lovellette[26], P. Lubrano[11,12], M. N. Mazziotta[14], J. E. McEnery[28,47], J. Mehault[19], P. F. Michelson[3], W. Mitthumsiri[3], T. Mizuno[48], A. A. Moiseev[47,49], C. Monte[13,14], M. E. Monzani[3], A. Morselli[30], I. V. Moskalenko[3], S. Murgia[3], M. Naumann-Godo[6], P. L. Nolan[3,68], J. P. Norris[50], E. Nuss[19], M. Ohno[51], T. Ohsugi[48], A. Okumura[3,52], N. Omodei[3], M. Orienti[29], E. Orlando[3], J. F. Ormes[53], M. Ozaki[51], D. Paneque[3,54], J. H. Panetta[3], D. Parent[1], M. Pesce-Rollins[5], M. Pierbattista[6], F. Piron[19], G. Pivato[10], H. Poon[10], T. A. Porter[3], D. Prokhorov[3], S. Rainò[13,14], R. Rando[9,10], M. Razzano[4,5], S. Razzaque[1], A. Reimer[3,55], O. Reimer[3,55], T. Reposeur[46], L. S. Rochester[3], M. Roth[56], H. F.-W. Sadrozinski[4], D. A. Sanchez[57], C. Sbarra[9], T. L. Schalk[4], C. Sgrò[5], G. H. Share[58,65], E. J. Siskind[59], G. Spandre[5], P. Spinelli[13,14], Ł. Stawarz[51,60], H. Takahashi[27], T. Tanaka[3], J. G. Thayer[3], J. B. Thayer[3], D. J. Thompson[28], L. Tibaldo[9,10], M. Tinivella[5], D. F. Torres[16,61], G. Tosti[11,12], E. Troja[28,69], Y. Uchiyama[3], T. L. Usher[3], J. Vandenbroucke[3], V. Vasileiou[19], G. Vianello[3,62], V. Vitale[30,63], A. P. Waite[3], P. Wang[3], B. L. Winer[36], D. L. Wood[64,65], K. S. Wood[26], Z. Yang[20,21], and S. Zimmer[20,21]

[1] Center for Earth Observing and Space Research, College of Science, George Mason University, Fairfax, VA 22030, USA
[2] Deutsches Elektronen Synchrotron DESY, D-15738 Zeuthen, Germany
[3] W. W. Hansen Experimental Physics Laboratory, Kavli Institute for Particle Astrophysics and Cosmology, Department of Physics and SLAC National Accelerator Laboratory, Stanford University, Stanford, CA 94305, USA; imos@stanford. edu
[4] Santa Cruz Institute for Particle Physics, Department of Physics and Department of Astronomy and Astrophysics, University of California at Santa Cruz, Santa Cruz, CA 95064, USA
[5] Istituto Nazionale di Fisica Nucleare, Sezione di Pisa, I-56127 Pisa, Italy
[6] Laboratoire AIM, CEA-IRFU/CNRS/Université Paris Diderot, Service d'Astrophysique, CEA Saclay, F-91191 Gif sur Yvette, France
[7] Istituto Nazionale di Fisica Nucleare, Sezione di Trieste, I-34127 Trieste, Italy
[8] Dipartimento di Fisica, Università di Trieste, I-34127 Trieste, Italy
[9] Istituto Nazionale di Fisica Nucleare, Sezione di Padova, I-35131 Padova, Italy
[10] Dipartimento di Fisica "G. Galilei," Università di Padova, I-35131 Padova, Italy
[11] Istituto Nazionale di Fisica Nucleare, Sezione di Perugia, I-06123 Perugia, Italy
[12] Dipartimento di Fisica, Università degli Studi di Perugia, I-06123 Perugia, Italy
[13] Dipartimento di Fisica "M. Merlin" dell'Università e del Politecnico di Bari, I-70126 Bari, Italy; nico.giglietto@ba.infn.it
[14] Istituto Nazionale di Fisica Nucleare, Sezione di Bari, I-70126 Bari, Italy
[15] Laboratoire Leprince-Ringuet, École polytechnique, CNRS/IN2P3, Palaiseau, France
[16] Institut de Ciències de l'Espai (IEEE-CSIC), Campus UAB, E-08193 Barcelona, Spain
[17] INAF-Istituto di Astrofisica Spaziale e Fisica Cosmica, I-20133 Milano, Italy
[18] ASI Science Data Center, I-00044 Frascati (Roma), Italy
[19] Laboratoire Univers et Particules de Montpellier, Université Montpellier 2, CNRS/IN2P3, Montpellier, France
[20] Department of Physics, Stockholm University, AlbaNova, SE-106 91 Stockholm, Sweden
[21] The Oskar Klein Centre for Cosmoparticle Physics, AlbaNova, SE-106 91 Stockholm, Sweden
[22] Agenzia Spaziale Italiana (ASI) Science Data Center, I-00044 Frascati (Roma), Italy
[23] IASF Palermo, I-90146 Palermo, Italy
[24] INAF-Istituto di Astrofisica Spaziale e Fisica Cosmica, I-00133 Roma, Italy
[25] Dipartimento di Fisica, Università di Udine and Istituto Nazionale di Fisica Nucleare, Sezione di Trieste, Gruppo Collegato di Udine, I-33100 Udine, Italy
[26] Space Science Division, Naval Research Laboratory, Washington, DC 20375-5352, USA
[27] Department of Physical Sciences, Hiroshima University, Higashi-Hiroshima, Hiroshima 739-8526, Japan
[28] NASA Goddard Space Flight Center, Greenbelt, MD 20771, USA
[29] INAF Istituto di Radioastronomia, I-40129 Bologna, Italy
[30] Istituto Nazionale di Fisica Nucleare, Sezione di Roma "Tor Vergata," I-00133 Roma, Italy
[31] Departamento de Física Teórica, Universidad Autónoma de Madrid, Cantoblanco, E-28049, Madrid, Spain
[32] Instituto de Física Teórica IFT-UAM/CSIC, Universidad Autónoma de Madrid, Cantoblanco, E-28049, Madrid, Spain
[33] Center for Space Plasma and Aeronomic Research (CSPAR), University of Alabama in Huntsville, Huntsville, AL 35899, USA
[34] School of Physics and Astronomy, University of Southampton, Highfield, Southampton SO17 1BJ, UK
[35] Centre d'Études Nucléaires de Bordeaux Gradignan, IN2P3/CNRS, Université Bordeaux 1, BP120, F-33175 Gradignan Cedex, France
[36] Department of Physics, Center for Cosmology and Astro-Particle Physics, The Ohio State University, Columbus, OH 43210, USA
[37] Osservatorio Astronomico di Trieste, Istituto Nazionale di Astrofisica, I-34143 Trieste, Italy
[38] Department of Physics, Royal Institute of Technology (KTH), AlbaNova, SE-106 91 Stockholm, Sweden
[39] Science Institute, University of Iceland, IS-107 Reykjavik, Iceland
[40] College of Science, Ibaraki University, 2-1-1, Bunkyo, Mito 310-8512, Japan
[41] Research Institute for Science and Engineering, Waseda University, 3-4-1, Okubo, Shinjuku, Tokyo 169-8555, Japan

[42] CNRS, IRAP, F-31028 Toulouse Cedex 4, France
[43] GAHEC, Université de Toulouse, UPS-OMP, IRAP, Toulouse, France
[44] Department of Astronomy, Stockholm University, SE-106 91 Stockholm, Sweden
[45] Istituto Nazionale di Fisica Nucleare, Sezione di Torino, I-10125 Torino, Italy
[46] Centre d'Études Nucléaires de Bordeaux Gradignan, Université Bordeaux 1, CNRS/IN2p3, F-33175 Gradignan, France
[47] Department of Physics and Department of Astronomy, University of Maryland, College Park, MD 20742, USA
[48] Hiroshima Astrophysical Science Center, Hiroshima University, Higashi-Hiroshima, Hiroshima 739-8526, Japan
[49] Center for Research and Exploration in Space Science and Technology (CRESST) and NASA Goddard Space Flight Center, Greenbelt, MD 20771, USA
[50] Department of Physics, Boise State University, Boise, ID 83725, USA
[51] Institute of Space and Astronautical Science, JAXA, 3-1-1 Yoshinodai, Chuo-ku, Sagamihara, Kanagawa 252-5210, Japan
[52] Solar-Terrestrial Environment Laboratory, Nagoya University, Nagoya 464-8601, Japan
[53] Department of Physics and Astronomy, University of Denver, Denver, CO 80208, USA
[54] Max-Planck-Institut für Physik, D-80805 München, Germany
[55] Institut für Astro- und Teilchenphysik and Institut für Theoretische Physik, Leopold-Franzens-Universität Innsbruck, A-6020 Innsbruck, Austria
[56] Department of Physics, University of Washington, Seattle, WA 98195-1560, USA
[57] Max-Planck-Institut für Kernphysik, D-69029 Heidelberg, Germany
[58] Department of Astronomy, University of Maryland, College Park, MD 20742, USA
[59] NYCB Real-Time Computing Inc., Lattingtown, NY 11560-1025, USA
[60] Astronomical Observatory, Jagiellonian University, 30-244 Kraków, Poland
[61] Institució Catalana de Recerca i Estudis Avançats (ICREA), Barcelona, Spain
[62] Consorzio Interuniversitario per la Fisica Spaziale (CIFS), I-10133 Torino, Italy
[63] Dipartimento di Fisica, Università di Roma "Tor Vergata," I-00133 Roma, Italy
[64] Praxis Inc., Alexandria, VA 22303, USA
Received 2012 May 4; accepted 2012 September 3; published 2012 October 9

ABSTRACT

We report on the detection of high-energy γ-ray emission from the Moon during the first 24 months of observations by the *Fermi* Large Area Telescope (LAT). This emission comes from particle cascades produced by cosmic-ray (CR) nuclei and electrons interacting with the lunar surface. The differential spectrum of the Moon is soft and can be described as a log-parabolic function with an effective cutoff at 2–3 GeV, while the average integral flux measured with the LAT from the beginning of observations in 2008 August to the end of 2010 August is $F(>100\ \mathrm{MeV}) = (1.04 \pm 0.01\ [\mathrm{statistical\ error}] \pm 0.1\ [\mathrm{systematic\ error}]) \times 10^{-6}\ \mathrm{cm}^{-2}\ \mathrm{s}^{-1}$. This flux is about a factor 2–3 higher than that observed between 1991 and 1994 by the EGRET experiment on board the *Compton Gamma Ray Observatory*, $F(>100\ \mathrm{MeV}) \approx 5 \times 10^{-7}\ \mathrm{cm}^{-2}\ \mathrm{s}^{-1}$, when solar activity was relatively high. The higher γ-ray flux measured by *Fermi* is consistent with the deep solar minimum conditions during the first 24 months of the mission, which reduced effects of heliospheric modulation, and thus increased the heliospheric flux of Galactic CRs. A detailed comparison of the light curve with McMurdo Neutron Monitor rates suggests a correlation of the trends. The Moon and the Sun are so far the only known bright emitters of γ-rays with fast celestial motion. Their paths across the sky are projected onto the Galactic center and high Galactic latitudes as well as onto other areas crowded with high-energy γ-ray sources. Analysis of the lunar and solar emission may thus be important for studies of weak and transient sources near the ecliptic.

Key words: astroparticle physics – gamma rays: general – Moon

Online-only material: color figures

1. INTRODUCTION

The brightest object in the night sky, the Moon has been studied by naked eyes for millennia and is well known to shine by reflected sunlight. At hard X-ray and γ-ray energies, the Moon shines as a result of cosmic-ray (CR) interactions with the lunar surface. Nuclear emission lines due to the spallation and activation of the surface material (regolith) by secondary neutrons as well as from natural radioactivity were first observed by γ-ray spectrometers on *Luna 10*, *11*, and *12* (Vinogradov et al. 1966, 1967) in the beginning of the space era and then by *Apollo 15* and *Apollo 16* missions (Metzger et al. 1973). These data provided the first insight into the chemical composition of the regolith. More recently, spatially resolved observations of the nuclear emission lines by the *Lunar Prospector* (e.g., Lawrence et al. 1998; Prettyman et al. 2006), *Kaguya* (Kobayashi et al. 2010), and *Chang'E-1* (Zhu et al. 2011) spacecraft were used to globally map the composition of the Moon.

The high-energy continuum γ-ray emission from the Moon was first detected by EGRET on the *Compton Gamma Ray Observatory* (which operated from 1991 to 2000). Early analysis of the 1991–1994 EGRET observations yielded the integral flux of the lunar emission of $F(E > 100\ \mathrm{MeV}) = (4.7 \pm 0.7) \times 10^{-7}\ \mathrm{cm}^{-2}\ \mathrm{s}^{-1}$ (Thompson et al. 1997), while a later reanalysis confirmed the detection and yielded a flux $F(E > 100\ \mathrm{MeV}) = (5.55 \pm 0.65) \times 10^{-7}\ \mathrm{cm}^{-2}\ \mathrm{s}^{-1}$ for the same viewing periods (Orlando & Strong 2008).

The steady continuum γ-ray emission of the solar system bodies arises from CR cascades developing in their surface layers. The principal emission processes are the decay of secondary neutral pions and kaons, produced by CRs hitting the surface, bremsstrahlung of primary and secondary electrons and positrons, and Compton scattering of the cascade photons. Although similar physical processes are involved for each body,

[65] Resident at Naval Research Laboratory, Washington, DC 20375, USA.
[66] Royal Swedish Academy of Sciences Research Fellow, funded by a grant from the K. A. Wallenberg Foundation.
[67] Funded by contract ERC-StG-259391 from the European Community.
[68] Deceased.
[69] NASA Postdoctoral Program Fellow, USA.

the observed γ-ray spectra are not the same owing to the different environments for development of CR cascades, such as the gaseous atmospheres of the Earth (N, O) (Abdo et al. 2009) and the Sun (H, He) (Abdo et al. 2011), and the atmosphereless surfaces of the Moon and asteroids. γ-ray emission lines have been observed from the rocky surfaces of Mars (Surkov et al. 1992; Boynton et al. 2007), Eros (Evans et al. 2001), Vesta (Prettyman et al. 2011), and Mercury (Rhodes et al. 2011), though the Moon is the best studied so far.

Calculations of interactions of CRs with the lunar surface are fairly straightforward, involving known physics processes, the well-measured spectrum and the composition of CRs near the Earth and composition of regolith, which was quite rigorously studied using the samples returned by the lunar missions as well as by remote sensing. The first calculation of the lunar γ-ray emission including a continuum spectrum above a few MeV was done by Morris (1984) using the CR spectrum, cross section data, and techniques available at that time. Recent detailed calculations were made by Moskalenko & Porter (2007) using the framework of the Geant4 particle interaction code (Agostinelli et al. 2003). The simulations show that the spectrum of γ-rays from the Moon is expected to be steep with an effective cutoff around 3–4 GeV (600 MeV for the inner part of the lunar disk) and exhibits a narrow pion-decay line at 67.5 MeV, perhaps unique in astrophysics. The emission from the limb of the Moon is expected to have a harder spectrum than that from the rest of the disk owing to the tangential directions of CR cascade development. Accurate measurements of the lunar emission can be used to test the details of the calculation with far better statistics and resolution than was possible with the previous EGRET observations.

So far the Moon, the Sun, and the Earth are the only observed emitters of high-energy (>100 MeV) γ-rays in the solar system. Searches for other potential sources or populations of sources, such as small asteroids and comets, in the solar system are also ongoing. Having solid surfaces composed of rock or ice, such objects may exhibit a spectrum similar to the lunar spectrum at high energies, which can be a useful template. Populations of such small objects, which are too small to be resolved individually, could be detectable in the Main Asteroid Belt, Kuiper Belt, Oort Cloud, and near the orbits of Jupiter and Neptune (Jovian and Neptunian Trojans; Moskalenko et al. 2008; Moskalenko & Porter 2009).

As the Moon moves across the sky, the flux and spectrum of the Moon are needed for analysis of γ-ray sources that it passes nearby. Although the motion of the Moon is fast compared to the integration times for most Large Area Telescope (LAT) source observations, it could affect analysis of flaring sources in close proximity.

In this paper, we report observations of the Earth-facing side of the Moon by the *Fermi*-LAT during first 24 months of the mission. During this period solar activity was extremely low, resulting in a high heliospheric flux of Galactic CRs. Therefore, the CR-induced γ-ray emission of the Moon was near its maximum. Preliminary results were reported by Giglietto (2009a, 2009b).

2. OBSERVATIONS AND DATA SELECTION

Fermi was launched on 2008 June 11 into circular Earth orbit with an altitude of 565 km and inclination of 25.°6 and an orbital period of 96 minutes. The principal instrument on *Fermi* is the LAT (Atwood et al. 2009), a pair-production telescope with a large effective area (~6500 cm^2 on-axis at 1 GeV based on post-launch Pass7 instrument response functions, IRFs) and field of view (2.4 sr or about 8×10^3 deg^2), sensitive to γ-rays between 20 MeV and >300 GeV. After the commissioning phase, the LAT began routine science operations on 2008 August 4. The *Fermi*-LAT normally operates in sky-survey mode where the whole sky is observed every two orbits.

Table 1
Summary of the Event Selection Cuts

Cumulative Event Selections	Photons (%)	Live Time (%)
$\theta_{\rm ROI} \leqslant 20^\circ$	100	100
$\lvert b_{\leftmoon} \rvert \geqslant 30^\circ$	48.8	56.6
$\theta_{\rm Sun} > 20^\circ$	43.5	50.2
$\theta(F_{\rm 1FGL} > 2 \times 10^{-7}$ cm^{-2} s$^{-1}) > 5^\circ$	40.1	46.8

The analysis presented here uses post-launch P7V6 Source class IRFs. These take into account pileup and accidental coincidence effects in the detector subsystems that were not considered in the definition of the pre-launch IRFs.[70] The new IRFs also have improved effective area at low energies while the point-spread function (PSF) has been adjusted based on in-flight measurements. The systematic uncertainty of the effective area for the Source class events is estimated as 10% at 100 MeV, decreasing to 5% at 560 MeV, and increasing to 20% at 10 GeV and above. The photon angular resolution is also energy dependent. The radius of the 68% containment region averaged over the LAT acceptance is about 4.°2 at 100 MeV, 2.°4 at 200 MeV, 1.°2 at 500 MeV, 0.°67 at 1 GeV, and 0.°18 at 10 GeV.

We use the LAT data collected between 2008 August 4 and 2010 August 31, with a total duration of about 24 months corresponding to solar minimum conditions. Our analysis of γ-ray emission from the Moon is similar to the analysis of quiescent solar emission described in Abdo et al. (2011). Events $\geqslant$100 MeV with a reconstructed direction within $\theta \leqslant 20^\circ$ from the position of the Moon (region of interest, ROI) and satisfying the Source class selection (Atwood et al. 2009) are used. To reduce the contamination from the γ-ray emission coming from CR interactions in Earth's upper atmosphere, our selection is refined by selecting events with zenith angles <100° and excludes time intervals when the ROI extends outside of this range. To reduce systematic uncertainties due to the bright diffuse γ-ray emission from the Galactic plane and a possible spillover due to the broad PSF at low energies, we have also excluded the data taken when the Moon was within 30° of the plane (requiring $\lvert b_{\leftmoon} \rvert \geqslant 30^\circ$). We further excluded the periods when the Moon was within 20° of the Sun (to exclude the brightest part of the extended emission due to the inverse Compton scattering of CR electrons off solar photons; Abdo et al. 2011) or within 5° of any other bright celestial source with integral flux $F_{\rm 1FGL} \geqslant 2 \times 10^{-7}$ cm^{-2} s^{-1} above 100 MeV as selected from the 1FGL *Fermi*-LAT source catalog (Abdo et al. 2010). These various selections produce a very clean event subsample, but at the expense of removing about 60% of the initial ROI data set as summarized in Table 1.

3. DATA ANALYSIS AND BACKGROUND EVALUATION

Analysis of the *Fermi*-LAT observations of the Moon involves aspects not part of a standard point-source analysis. (1) The Moon moves across the sky rapidly, covering more than 10° per

[70] Details on the pre-launch instrument performance can be found in the *Fermi*-LAT calibration paper (Atwood et al. 2009).

day, and so the background for the source analysis is constantly changing. (2) The Moon is close enough to the Earth that parallax due to the motion of the *Fermi* spacecraft produces an apparent motion of the source relative to the fixed stars of up to 0.°6 in an orbit. (3) The Moon is not a point source. It subtends ∼0.°5 on the sky. Such source extension, however, is measurable by the LAT only at energies above several GeV where the PSF is sufficiently small. At lower energies where most of the LAT photons are detected, a point-like source approximation is expected to be adequate.

A dedicated set of tools was developed, not a part of the standard *Fermi*-LAT Science Tools package, to deal with moving sources such as the Moon and the Sun. Using these specialized tools, the data are selected in a moving frame centered on the instantaneous lunar position, which takes into account the parallax corrections and is computed using the JPL ephemeris libraries.[71] More details on the analysis of moving sources can be found in the paper by Abdo et al. (2011) dedicated to the analysis of the γ-ray emission from the quiet Sun.

For the analysis of the Moon-centered maps, we used the *Fermi*-LAT Science Tools[72] version 9r23p1. The *gtlike* tool provides maximum likelihood parameter values (using the method described in Cash 1979; Strong 1985; Mattox et al. 1996), which derives error estimates (and a full covariance matrix) from Minuit,[73] a minimization tool supported by CERN, using the quadratic approximation around the maximum likelihood fit.

As a first step, we verify the analysis procedure using simulated point-like sources with the computed spectra corresponding to (1) the inner part of the lunar disk (the total minus the limb emission), giving a softer spectrum, and to (2) the total flux, which has a harder spectrum (Moskalenko & Porter 2007). The analysis was done in Moon-centered coordinates using the same analysis chain and the same set of cuts as applied to the real data. Figure 1 shows the predicted differential γ-ray flux for the inner part of the lunar disk and for the total emission corresponding to the solar minimum conditions together with the reconstructed spectra (points). The results demonstrate an excellent agreement between the reconstructed and simulated spectra.

For a moving source evaluation of the background is of primary importance. The main components of the background emission are the diffuse Galactic and isotropic (presumably extragalactic) emission, weak point sources, and the instrumental background (such as, e.g., misidentified CR particles). The evaluation of the background is made using the "fake-source" method described in detail in Abdo et al. (2011). For this method, we apply to an imaginary source that follows the path of the Moon the same cuts as used for the Moon itself. Analysis of this "fake-Moon" yields an estimate of the background. To reduce statistical errors in the background determination, the background is averaged over four fake-Moon sources displaced from each other and from the Moon itself by 30° intervals along the ecliptic. Because all fake-Moon sources are trailing the Moon at different angular distances over a period of 24 months, i.e., more than 24 full sidereal periods, they are sampling the same area on the sky. The background fluxes determined using individual fake-Moon sources are consistent within a fraction of a percent. Note that the 24 month analysis period is long enough

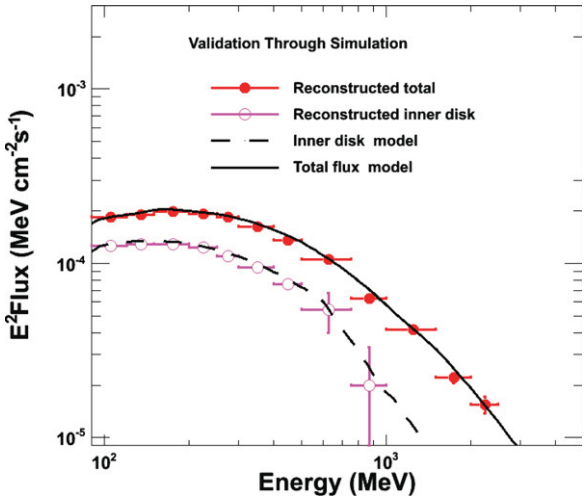

Figure 1. Verification of the analysis procedure for a moving source. Lines: predicted (Moskalenko & Porter 2007) differential γ-ray flux for the inner part of the lunar disk (dashes, the total minus limb emission) and for the total emission (solid) corresponding to solar minimum conditions. Data points: reconstructed spectra from the *simulated* source. Open magenta circles—the central part of the disk and filled red points—total emission.

(A color version of this figure is available in the online journal.)

to average out any effects connected with incomplete sampling of the background. Attenuation of the diffuse background due to the shielding by the lunar disk itself is negligible compared to the observed flux because the solid angle subtended by the Moon is so small.

4. RESULTS

An ROI of 20° radius around the position of the Moon was selected, which is sufficiently wide to account for the broad LAT PSF at ∼100 MeV (Atwood et al. 2009). Figure 2 shows the count profiles for events with $E = 100$ MeV–10 GeV within 10° of the Moon as a function of right ascension (α) and declination (δ) offsets with respect to the center of the lunar disk. It also shows the count distributions for the average fake-Moon and a sample of data simulated using a point-like source model. The simulation has been performed with the *gtobssim* simulator (LAT Science Tools), a standard tool for simulation of the γ-ray sky.

The angular size of the Moon[74] is ∼0.°5. In order to test the possible effects of the finite angular size we plot the density of the events (100 MeV–10 GeV) around the Moon versus the angular distance from the center of the disk (Figure 3). Also shown are the event distributions found for the fake-Moon and simulated results for a point-like source with the spectrum matching the lunar spectrum. The event density has been computed as the number of observed events per annulus centered at the Moon position and normalized by the subtended solid angle. As expected, the angular size of the Moon has no effect on the angular profile of observed events due to the broad PSF of the lower-energy γ-rays that dominate the data set.

The distribution for a simulated source in Figures 2 and 3 looks somewhat wider than the data, most likely due to deviations of the observed spectrum from the log-parabola fit (details of the fitting procedure are given below). Indeed, in Figure 4 (left), the log-parabola fit seems to give a smaller number of

[71] http://iau-comm4.jpl.nasa.gov/access2ephs.html
[72] Available from Fermi Science Support Center (FSSC), http://fermi.gsfc.nasa.gov/ssc
[73] http://seal.web.cern.ch/seal/work-packages/mathlibs/minuit/home.html
[74] Variations of the apparent size of the lunar disk due to its elliptical orbit average out over a time interval of about a month.

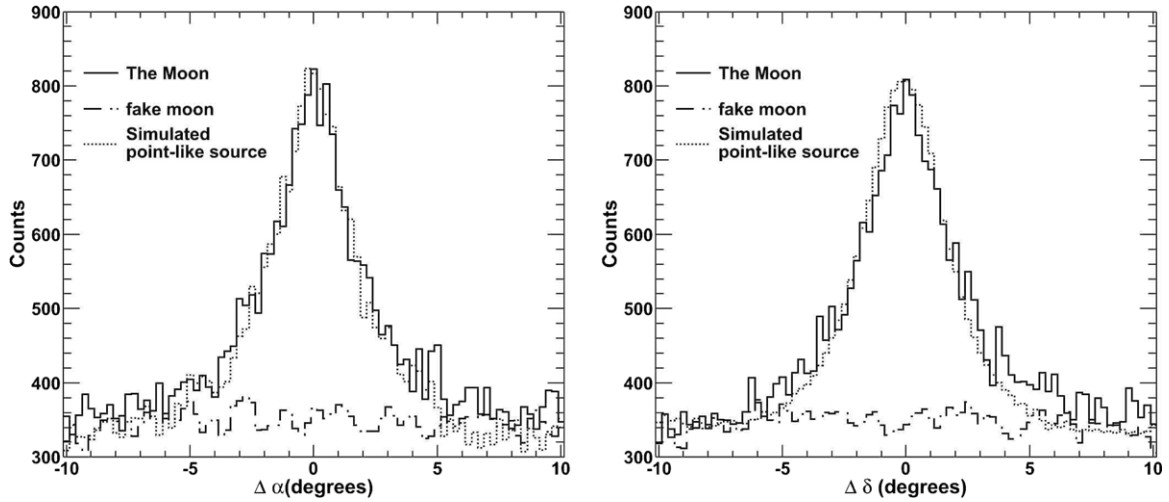

Figure 2. Observed count profiles within 10° radius centered at the position of the Moon. The observed events are selected in the energy range 100 MeV–10 GeV and projected onto the α (left) or δ (right) offsets relative to the nominal position. Also shown are the count distribution observed for the fake-Moon and the simulation for a point-like source having the same observed spectrum.

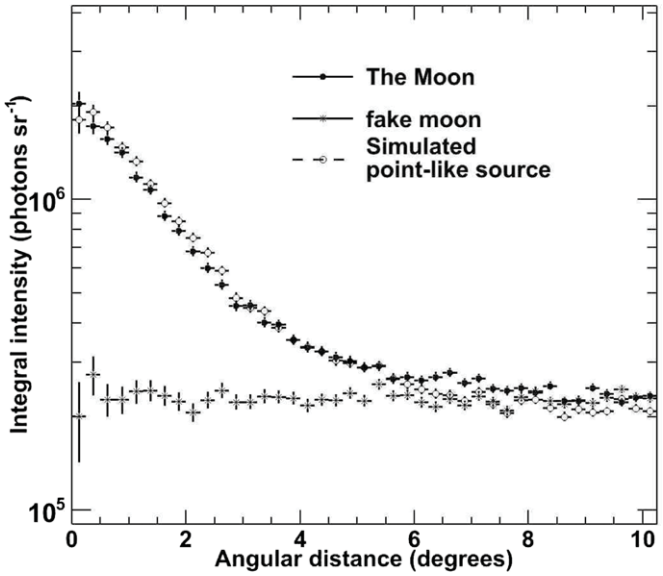

Figure 3. Event density vs. the angular distance from the center of the Moon for photons in the energy range 100 MeV–10 GeV. The angular distance scale shows the inner radius of each annulus while the width of the annulus was fixed at 0.°25 and the points are plotted at the mid-point radius of each annulus. Also shown are the count distributions observed for the fake-Moon and the simulation for a point-like source having the same observed spectrum.

events than the observed spectrum at low energies. Since the integral flux of the simulated source matches the integral flux of the real source, this, combined with the energy dependence of the PSF, leads to shorter tails for the simulated distribution and somewhat higher flux at the core. The full maximum likelihood analysis of the data sample indicates that the maximum of the emission is centered at the computed position of the Moon, with a 68% confidence level error radius of 0.°03.

In order to derive the energy spectrum of the Moon, we determined the background intensity using the previously described fake-Moon analysis, where we applied the same data selections that were used for the real Moon. The background was not allowed to vary in the likelihood analysis. Figure 4 shows the spectrum of the Moon, compared with past observations and theoretical predictions. The observed spectrum was fit with a simple power law and a log-parabolic function. The log-parabolic function

$$dN/dE = N_0(E/E_b)^{-\alpha-\beta\log(E/E_b)}, \quad (1)$$

provides the best test statistic[75] (TS). Here $N_0 = (70 \pm 6) \times 10^{-9}$ cm^{-2} s^{-1} MeV^{-1}, $\alpha = 1.39 \pm 0.07$, $\beta = 0.45 \pm 0.02$, and $E_b = 44.2 \pm 2.3$ MeV. This yields the integral flux $F(>100$ MeV$) = (1.04 \pm 0.01\,[\text{stat}] \pm 0.1\,[\text{syst}]) \times 10^{-6}$ cm^{-2} s^{-1} for a point-like source at the expected position, where the two uncertainties are statistical and systematic. Note that the parameters of the log-parabolic function and their errors are not independent; therefore, the relative statistical error of the integral flux is significantly smaller than the relative errors of individual parameters.

The systematic error shown above has been evaluated by repeating the fit with the normalization of the background derived from the fake-Moon analysis left as a free parameter. It was found that in this case the normalization of the modeled background emission changes by $\lesssim$1%. The systematic error also includes the effect of uncertainties in the effective area at low energies.

In addition to the spectral fit covering the full energy range, we constructed the spectrum for logarithmically spaced energy bins using the *gtlike* tool. For the fluxes in finite energy ranges, separate likelihood analyses were made for each range, with a power-law spectral model. Table 2 shows the differential flux, which was determined from the observed flux in the given energy range by dividing by the corresponding energy interval. The table also shows corresponding statistical errors and the TS values. Only an upper limit is shown for the entry with TS < 10.

Since the γ-ray emission of the Moon is induced by CR interactions, it should correlate with the ground neutron monitor (NM) rates, which measure the integral intensity of Galactic CRs. On the other hand, it should anti-correlate with the maximum extent of the heliospheric current sheet (tilt angle) that has been used in modulation models as a proxy for solar activity since the 1970s (e.g., Potgieter 2008).

To test the correlation, the whole period of observations was divided into two-month intervals, which are long enough to keep the statistical error sufficiently low (Table 3). Figure 5

[75] The likelihood test statistic, TS = 2Δlog(likelihood), between models with and without the source is defined in Mattox et al. (1996).

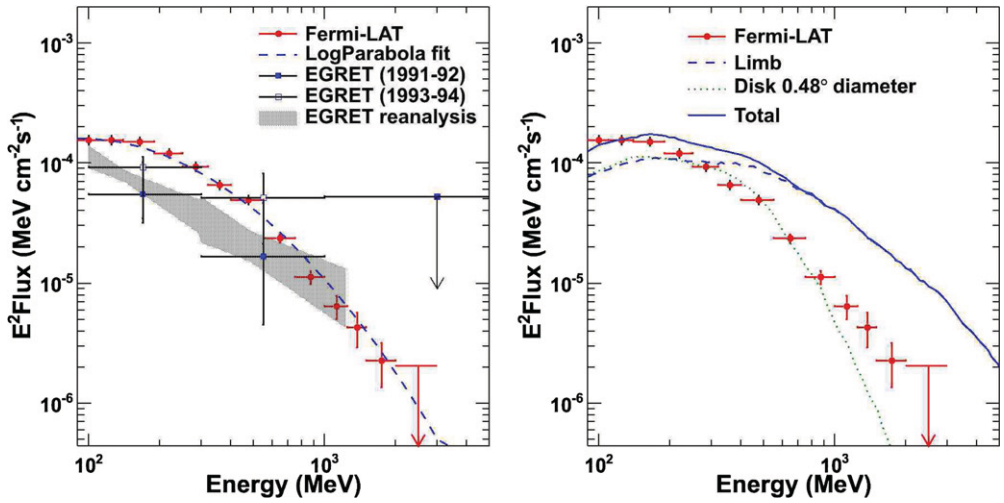

Figure 4. Left: γ-ray spectrum of the Moon derived from the first 24 months of observations by the *Fermi*-LAT (red filled circles) and the fitted log-parabolic function Equation (1) (black dashed line). The blue squares show the EGRET data corresponding to periods of lower (open squares, EGRET Low) and higher (filled squares, EGRET High) solar activity, respectively (Thompson et al. 1997). The gray shaded region is the result of the reanalysis of the EGRET data (1991–1995) by Orlando & Strong (2008). Right: LAT spectrum compared with the predicted spectrum (Moskalenko & Porter 2007) corresponding to the period of low solar activity (solid line). The dotted and dashed blue lines show the separate spectra from the inner part of the lunar disk (0.°48 diameter) and the limb, respectively, assuming an average diameter of 0.°52.

(A color version of this figure is available in the online journal.)

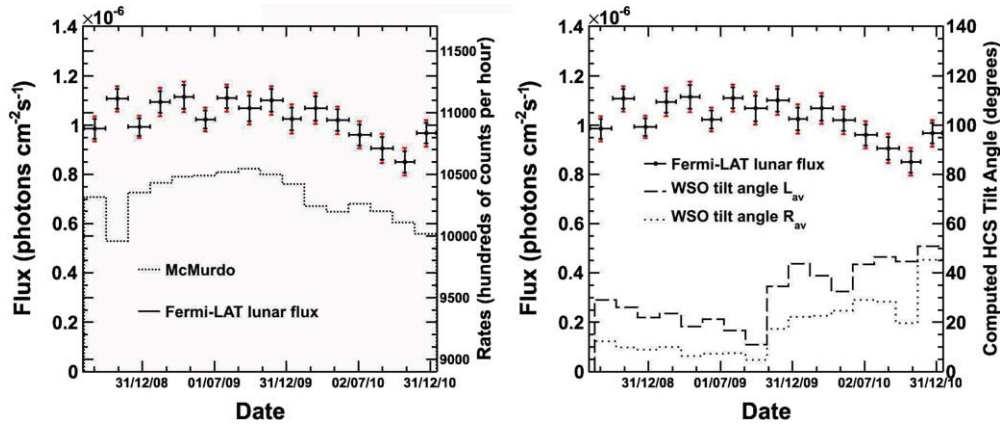

Figure 5. Integral γ-ray flux (>100 MeV) observed during the first 30 months (same selection cuts as in Figure 4) in two-month intervals compared with the McMurdo NM rates (left panel) and heliospheric current sheet tilt angles (right panel) for two Hoeksema models (e.g., Hoeksema 1992; Zhao & Hoeksema 1995), the classic L model (dashed line) and a newer R model (dotted line). L_{av} and R_{av} are the averages of the tilt angles calculated for the northern and southern hemispheres. Systematic errors in the photon flux are shown in black, and statistical errors are in red. The NM rates are corrected for the site air pressure.

(A color version of this figure is available in the online journal.)

Table 2
The Observed Spectrum of the Moon

Energy Interval (MeV)	Differential Flux ± Stat ± Syst (cm^{-2} s^{-1} MeV^{-1})	TS
90–110	$(1.57 \pm 0.06 \pm 0.16) \times 10^{-8}$	1577
110–140	$(1.01 \pm 0.03 \pm 0.1) \times 10^{-8}$	2746
140–190	$(5.7 \pm 0.1 \pm 0.5) \times 10^{-9}$	4576
190–250	$(2.54 \pm 0.07 \pm 0.2) \times 10^{-9}$	3469
250–320	$(1.16 \pm 0.04 \pm 0.1) \times 10^{-9}$	2356
320–400	$(5.1 \pm 0.2 \pm 0.1) \times 10^{-10}$	1449
400–550	$(2.2 \pm 0.1 \pm 0.1) \times 10^{-10}$	1395
550–750	$(5.7 \pm 0.4 \pm 0.3) \times 10^{-11}$	464
750–1000	$(1.5 \pm 0.2 \pm 0.08) \times 10^{-11}$	158
1000–1250	$(5 \pm 1 \pm 0.3) \times 10^{-12}$	49
1250–1500	$(2.3 \pm 0.7 \pm 0.1) \times 10^{-12}$	25
1500–2000	$(8 \pm 3 \pm 0.5) \times 10^{-13}$	14
2000–3000	u.l. 90% c.l. 3.4×10^{-13}	<10

(left) shows the observed lunar flux in each sub-period together with the two-month averaged rates from the McMurdo NM[76] in Antarctica, which has a low geomagnetic cutoff. There is a tentative correlation of the trends, with the rates slowly rising from the beginning of observations until the end of 2009 December. A ∼5% drop in the NM rates in 2010 corresponds to a ∼10%–15% drop in the observed lunar flux. Figure 5 (right) shows the observed lunar flux in each sub-period together with the tilt angle[77] for two of Hoeksema's models (e.g., Hoeksema 1992; Zhao & Hoeksema 1995). The upper and lower histograms represent his old (L model) and new model (R model), respectively. The difference between the models illustrates the systematic error associated with determination of the tilt angles. There is a hint of an anti-correlation of the observed lunar flux with the solar activity. These comparisons

[76] Operated by Bartol Research Institute, http://neutronm.bartol.udel.edu
[77] http://wso.stanford.edu/Tilts.html

Table 3
The Observed Light Curve of the Moon

Time Interval, MJD	Integral Flux ($E > 100$ MeV) ± Stat ± Syst ($\times 10^{-7}$ cm^{-2} s^{-1})
54682.7–54736.7	9.9 ± 0.4 ± 1.0
54740.0–54794.6	11.1 ± 0.4 ± 1.0
54794.7–54850.7	9.9 ± 0.4 ± 1.0
54850.7–54901.2	11.3 ± 0.4 ± 1.0
54911.9–54960.4	11.1 ± 0.5 ± 1.0
54966.6–55014.8	10.2 ± 0.4 ± 1.0
55021.1–55069.4	11.1 ± 0.4 ± 1.0
55075.6–55130.6	10.7 ± 0.5 ± 1.0
55130.7–55186.6	11.0 ± 0.5 ± 1.0
55186.7–55233.3	10.2 ± 0.5 ± 1.0
55243.0–55298.7	10.7 ± 0.5 ± 1.0
55298.7–55354.6	10.2 ± 0.4 ± 1.0
55354.7–55410.6	9.6 ± 0.4 ± 1.0
55410.7–55466.6	9.1 ± 0.5 ± 0.9
55472.3–55521.2	8.5 ± 0.4 ± 0.9
55521.2–55576.0	9.7 ± 0.4 ± 1.0

illustrate the expected dependence of the observed γ-ray flux on the CR flux as measured by the NM, and on the solar activity as traced by the tilt angle, but the dynamic range in this study is too limited to make a definitive conclusion.

5. DISCUSSION AND CONCLUSION

For the first time the γ-ray spectrum of the Moon is measured with high statistical precision between ~100 MeV and 2 GeV. The observed spectrum is somewhat softer than expected (Moskalenko & Porter 2007) and matches fairly well the predicted soft spectrum of the central part of the disk above 200 MeV. Predicted spectra shown in Figure 4 (right) are from a new calculation that employs the code developed by Moskalenko & Porter (2007), but shows the emission from the inner part of the disk with the diameter of 0.°48. This calculation was selected as the best match for the observed spectrum. The limb does not seem to give a significant contribution to the total flux, except below 200 MeV and above ~1 GeV, where the inner disk spectrum exhibits a cutoff. At low energies ($\lesssim$200 MeV), the calculated total flux agrees well with the observations. This is because the angular distribution of the CR-induced γ-ray emission is broad at low energies and there is essentially no distinction between the inner disk and the limb (dashed and dotted lines).

Although the LAT cannot separately measure the disk and limb spectra, we assume that the spectral discrepancy originates from an overestimate of the limb contribution. We therefore consider a possible deficiency in the modeling. In particular, the effect of the roughness of the lunar surface was not considered in earlier modeling, which assumed a smooth surface. The relevant size scale for γ-ray production is the particle interaction length, which is ~90 g cm^{-2} for GeV protons in oxygen (the most abundant element in Moon rock). The latter corresponds to ~50 cm for lunar regolith (density ~1.8 g cm^{-3}), implying that the distribution of intermediate-sized rocks and boulders is the most important factor. Attenuation by this surface debris of the flux of CR particles coming from tangential directions would result in a softer γ-ray spectrum resembling the observations, while the emission produced by CRs with larger incident angles is less affected.

Physical properties of the Moon surface have been a matter of practical interest since the glorious days of early space exploration and the beginning of robotic (Lunokhod 1 and Lunokhod 2) and human (the *Apollo* Lunar Roving Vehicles) transportation on the lunar surface (see, e.g., Heiken et al. 1991). Recent measurements by the Lunar Orbiter Laser Altimeter (Rosenburg et al. 2011) allowed a systematic evaluation of the lunar surface roughness to be done for the first time. It was found that most of the surface is characterized by a fractal-like roughness. This information can be used for a description of the surface characteristics for a future realistic modeling of CR interactions with the lunar surface.

A comparison of *Fermi*-LAT and EGRET observations shows clear evidence of an anti-correlation of the lunar γ-ray flux with the level of solar activity. Subdivision of the EGRET data into two samples, data taken during the solar maximum 1991–1992 and data taken during the period of moderate activity 1993–1994, indicated integral fluxes of 3.5×10^{-7} cm^{-2} s^{-1} and 7×10^{-7} cm^{-2} s^{-1}, respectively, suggesting that the γ-ray flux is higher when solar activity is lower (Thompson et al. 1997). The LAT observations came at a time of extremely low solar activity, and the 2008–2010 LAT flux is higher than any of the EGRET results, confirming the trend.

During the period reported in this paper, the McMurdo NM rates were up to 50% higher than the rates reported during the EGRET mission (Thompson et al. 1997). Correspondingly, the analysis of the *Fermi*-LAT data yields for the integral lunar flux $F(> 100$ MeV$) = 1.04 \pm 0.02$ [stat] $\pm$ 0.2 [syst] $\times 10^{-6}$ cm^{-2} s^{-1}, about a factor of two increase over the EGRET flux averaged over all periods of observations ($\sim 5 \times 10^{-7}$ cm^{-2} s^{-1}), in reasonable agreement with predictions for the CR environment associated with low solar activity. A comparison of the LAT light curve with the McMurdo NM rates shows a tentative correlation with the NM rates tracing the integral flux of Galactic CRs and a provisional anti-correlation with the tilt angle of the heliospheric current sheet, which is a proxy for the solar activity. Future LAT observations of variations of the lunar γ-ray flux over a significant part of the solar cycle are necessary to clearly establish the correlation/anti-correlation.

The *Fermi*-LAT observations of the Moon have provided detailed flux and spectral information that can be used to compare with future, more detailed models. They can also serve as a useful template to search for emission from populations of small bodies in the solar system (Moskalenko et al. 2008) and are available for analysis of LAT sources that are close to the Moon during flaring activity. Although indirect, the lunar γ-rays offer the advantage of monitoring the CR flux outside Earth's geomagnetic field.

The *Fermi*-LAT Collaboration acknowledges generous ongoing support from a number of agencies and institutes that have supported both the development and the operation of the LAT as well as scientific data analysis. These include the National Aeronautics and Space Administration and the Department of Energy in the United States, the Commissariat à l'Energie Atomique and the Centre National de la Recherche Scientifique/Institut National de Physique Nucléaire et de Physique des Particules in France, the Agenzia Spaziale Italiana and the Istituto Nazionale di Fisica Nucleare in Italy, the Ministry of Education, Culture, Sports, Science and Technology (MEXT), High Energy Accelerator Research Organization (KEK), and Japan Aerospace Exploration Agency (JAXA) in Japan, and the K. A. Wallenberg Foundation, the Swedish Research Council, and the Swedish National Space Board in Sweden.

Additional support for science analysis during the operations phase is gratefully acknowledged from the Istituto Nazionale di Astrofisica in Italy and the Centre National d'Études Spatiales in France. I.V.M. acknowledges support from NASA Grant NNX11AQ06G.

REFERENCES

Abdo, A. A., Ackermann, M., Ajello, M., et al. 2009, Phys. Rev. D, 80, 122004
Abdo, A. A., Ackermann, M., Ajello, M., et al. 2010, ApJS, 188, 405
Abdo, A. A., Ackermann, M., Ajello, M., et al. 2011, ApJ, 734, 116
Agostinelli, S., Allison, J., Amako, K., et al. 2003, Nucl. Instrum. Meth., A506, 250
Atwood, W. B., Abdo, A. A., Ackermann, M., et al. 2009, ApJ, 697, 1071
Boynton, W. V., Taylor, G. J., Evans, L. G., et al. 2007, J. Geophys. Res. (Planets), 112, 12
Cash, W. 1979, ApJ, 228, 939
Evans, L. G., Starr, R. D., Brückner, J., et al. 2001, Meteorit. Planet. Sci., 36, 1639
Giglietto, N. for the *Fermi*-LAT Collaboration. 2009a, Proc. 31st ICRC (Łodz), arXiv:0907.0541
Giglietto, N. for the *Fermi*-LAT Collaboration. 2009b, arXiv:0912.3734
Heiken, G. H., Vaniman, D. T., & French, B. M. 1991, Lunar Sourcebook—A User's Guide to the Moon (Cambridge: Cambridge Univ. Press)
Hoeksema, J. T. 1992, in Solar Wind Seven Colloquium, ed. E. Marsch & R. Schwenn (New York: Pergamon Press), 191
Kobayashi, S., Hasebe, N., Shibamura, E., et al. 2010, Space Sci. Rev., 154, 193
Lawrence, D. J., Feldman, W. C., Barraclough, B. L., et al. 1998, Science, 281, 1484
Mattox, J. R., Bertsch, D. L., Chiang, J., et al. 1996, ApJ, 461, 396
Metzger, A. E., Trombka, J. I., Peterson, L. E., Reedy, R. C., & Arnold, J. R. 1973, Science, 179, 800
Morris, D. J. 1984, J. Geophys. Res., 89, 10685
Moskalenko, I. V., & Porter, T. A. 2007, ApJ, 670, 1467
Moskalenko, I. V., & Porter, T. A. 2009, ApJ, 692, L54
Moskalenko, I. V., Porter, T. A., Digel, S. W., Michelson, P. F., & Ormes, J. F. 2008, ApJ, 681, 1708
Orlando, E., & Strong, A. W. 2008, A&A, 480, 847
Potgieter, M. S. 2008, J. Atmos. Sol.-Terr. Phys., 70, 207
Prettyman, T. H., et al. 2006, J. Geophys. Res. (Planets), 111, 12007
Prettyman, T. H., Feldman, W. C., McSween, H. Y., et al. 2011, Space Sci. Rev., 163, 371
Rhodes, E. A., Evans, L. G., Nittler, L. R., et al. 2011, Planet. Space Sci., 59, 1829
Rosenburg, M. A., Aharonson, O., Head, J. W., et al. 2011, J. Geophys. Res. (Planets), 116, E02001
Strong, A. W. 1985, A&A, 150, 273
Surkov, I. A., Moskaleva, L. P., Khariukova, V. P., et al. 1992, Kosmicheskie Issledovaniia, 30, 262
Thompson, D. J., Bertsch, D. L., Morris, D. J., & Mukherjee, R. 1997, J. Geophys. Res., 102, 14735
Vinogradov, A. P., Surkov, Y. A., Chernov, G. M., Kirnozov, F. F., & Nazarkina, G. B. 1966, Cosm. Res., 4, 751
Vinogradov, A. P., Surkov, Y. A., Chernov, G. M., Kirnozov, F. F., & Nazarkina, G. B. 1967, Cosm. Res., 5, 741
Zhao, X., & Hoeksema, J. T. 1995, Adv. Space Res., 16, 181
Zhu, M.-H., Ma, T., Chang, J., et al. 2011, Sci. China G, 54, 2083